ISIJ International, Vol. 57 (2017), No. 7, pp. 1268–1272

Difference in Reheat Cracking Susceptibility of 2.25Cr-W and 9Cr-W Heat-resistant Steels

Hyun Je SUNG, Nam Hoe HEO* and Sung-Joon KIM

Graduate Institute of Ferrous Technology, POSTECH, Pohang, 37673 Republic of Korea.

(*Received on December 22, 2016; accepted on March 21, 2017*)

This research has been performed to evaluate the reheat cracking susceptibility of 9Cr T/P92 heat-resistant steels and find the difference in susceptibility between 2.25Cr T/P23 and 9Cr T/P92 heat-resistant steels. After the welding simulation at 1 200°C and 1 300°C, the prior austenite grain size is much smaller in the T/P92 steel than the T/P23 steel. This is attributed to the undissolved Nb-rich carbo-nitrides in the T/P92 during the welding simulation which inhibit the growth of prior austenite grains. After tensile test at 750°C for the evaluation of cracking susceptibility, the fracture mode is typically intergranular in the T/P23 steel, while that of the T/P92 is ductile. Therefore, the insensitivity to intergranular cracking of the T/P92 steel is mainly attributed to the much lower phosphorus segregation concentration at grain boundaries which is caused by the smaller prior austenite grain size. Calculation results finally confirm that the grain boundary segregation concentration of phosphorus decreases with decreasing grain size.

KEY WORDS: intergranular cracking; prior-austenite grain size; carbo-nitrides; martensitic heat-resistant steels.

1. Introduction

Intergranular reheat cracking occurs in the coarse-grained heat affected zone (CGHAZ) of weldment after post-weld heat treatment (PWHT) or under the service condition.[1,2] It has been suggested that the reheat cracking is attributed to grain interiors strengthened by MX precipitates and soft prior austenite grain boundaries (PAGBs) resulting from the depletion of alloying elements.[3–6] During exposure to high temperature, the thermal stress is concentrated at the soft denuded zone, causing the intergranular cracking in which the revealed PAGBs surfaces include dimples considered as micro-ductile fracture areas.[7–9] On the other hand, lots of studies have supported that the segregation of impurities (especially, phosphorus) to the PAGBs causes the intergranular cracking by lowering the cohesive grain boundary strength.[10–23] The T/P23 heat-resistant steel (2.25Cr1.5WVNb) has been known to show a high susceptibility to the reheat cracking. Meanwhile, the T/P92 heat-resistant steel (9Cr1.5W0.5MoVNb) is not susceptible to the reheat cracking.[1,2]

It is the purpose of this research to investigate the reason for the difference in intergranular cracking susceptibility of T/P23 and T/P92 heat-resistant steels.

2. Experimental Procedure

T/P23[23] and T/P92 heat-resistant steels were prepared using vacuum induction melting. The chemical compositions of the steels were analyzed by the optical emission spectrometer (OES, OBLF QSN-750) and are shown in **Table 1**. These compositions follow American Society for Testing and Materials (ASTM) A213-T23 and A213-T92. The ingots were homogenized at 1 200°C for 1 hour and hot-rolled to 12 mm thick plates. Rectangular bars with a dimension of 11 × 11 × 150 mm^3 were machined from the plates in the hot-rolling direction. These bars were given to a heat treatment at 1 050°C for 1 hour which was followed by air cooling and subsequently tempered at 750°C for 0.5 hour under an argon atmosphere. After the heat treatment, tensile specimens of 8 mm gauge length and 7 mm gauge diameter were machined from the rectangular bars.

Reheat cracking observed just after the PWHT was simulated by a thermo-mechanical simulator (FDC, THERMECMASTOR-Z). The gauge part of each specimen was induction-heated to 1 200°C and 1 300°C at a heating rate of 25°C/s which is the limit heating rate for the precise temperature control. After holding at the temperature for 5 seconds, the specimen was fast cooled to room temperature by helium gas. The specimens were again heated to 750°C which is usually the post-weld heat treatment (PWHT) temperature at a heating rate of 10°C/s. As soon as the temperature reached 750°C, the tensile test was carried out on the specimen without holding at the temperature at a cross-head speed of 0.5 mm/min. During tests, an inert argon atmosphere was maintained to minimize oxidation of specimens. After the tensile test, the specimen was fast cooled to room temperature with helium gas.

The microstructure and chemical information of phases were examined by a field-emission scanning electron microscope (FE-SEM, ZEISS ULTRA-55) at 10 kV and field-emission transmission electron microscope (FE-TEM, JEOL

* Corresponding author: E-mail: nhheo@postech.ac.kr
DOI: http://dx.doi.org/10.2355/isijinternational.ISIJINT-2016-737

JEM-2100F) equipped with an energy-dispersive spectroscope (EDS, OXFORD) at 200 kV. Fracture surfaces and reduction of area (RA) were investigated, using the FE-SEM after ultrasonic cleaning of specimens in acetone. In order to find high-angle PAGBs, electron backscatter diffraction (EBSD, FEI QUANTA 3D FEG) measurement was carried out using a FE-SEM equipped with a TSL orientation imaging microscopy system at 20 kV. Carbon distribution depending on phases was examined by a field-emission electron probe micro-analyzer (FE-EPMA, JEOL JXA-8530F) at 15 kV. Hardness was measured with a Vickers indenter (Mitutoyo HM-200) using a force of 500 gf and a dwell time of 10 seconds.

The interfacial segregation behavior of solutes was investigated, using an Auger electron spectroscope (AES, PHI 700). The AES specimens were machined from the tensile tested specimens in the tensile stress direction. They were chilled with liquid nitrogen in the AES for 1 hour and in-situ fractured in ultra-high vacuum of 9×10^{-8} Pa or better. Typical parameters were the primary electron beam energy of 5 kV and an electron beam size of about 200 nm. About twenty points of grain boundaries were chosen for the AES analysis, respectively. The AES peaks of Fe_{703} and P_{120} were used, and the peak to peak height ratios (PHR, I/I_{Fe}) obtained from the differential AES spectra were averaged.

3. Results

In order to predict phases formed during heat treatments and welding simulations, the equilibrium phase fractions are calculated by Thermo-Calc using the TCFE7 database and the results are shown in **Fig. 1**. The Nb-rich MX carbo-nitrides in the T/P92 specimen are not dissolved into the matrix up to about 1 285°C. As shown in **Fig. 2**, some undissolved Nb-rich MX carbo-nitrides remain in the T/P92 steel

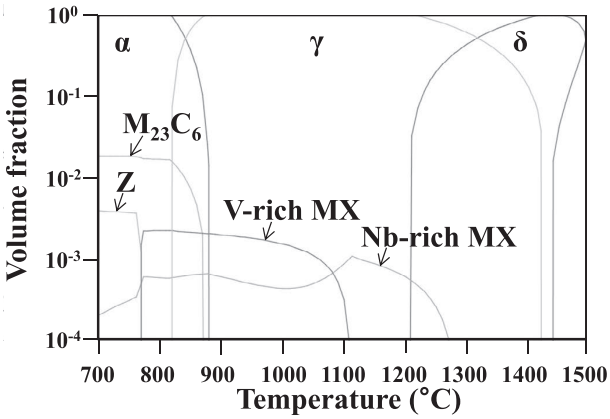

Fig. 1. The equilibrium phase fractions in T/P92 steel calculated by Thermo-Calc using the TCFE7 database.

Table 1. Chemical compositions of the prepared samples (wt.%).

	C	Si	Mn	P	S	Ni	Cr	Mo	V	Nb	W	N	Fe
T/P23[23]	0.10	0.32	0.54	0.01	<0.002	–	2.27	–	0.26	0.05	1.47	0.01	Balance
T/P92	0.08	0.38	0.50	0.01	<0.002	0.20	8.58	0.52	0.19	0.10	1.50	0.05	Balance

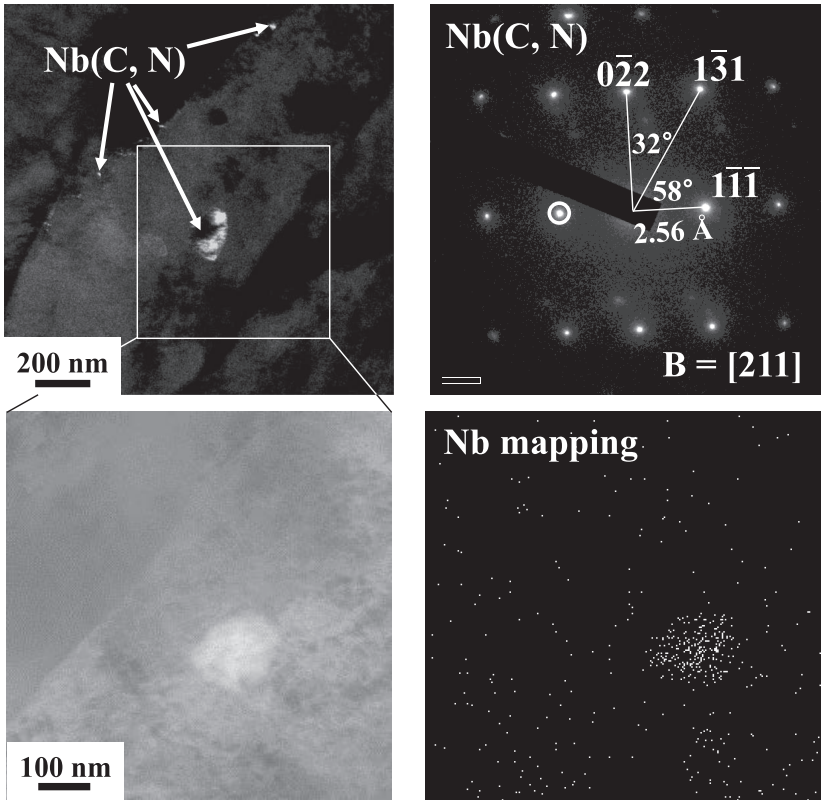

Fig. 2. Dark field image, diffraction pattern, scanning transmission electron microscopy-high angle annular dark field (STEM-HAADF) and energy-dispersive spectroscopy (EDS) mapping images of welding-simulated T/P92 specimen at a peak temperature of 1 200°C.

after the welding simulation at 1 200°C. Moreover, δ-ferrite can be formed after the welding simulation at 1 300°C in the T/P92 steel, due to the relatively high chromium content.

Changes in prior austenite grain size of the T/P92 steel and phases with welding simulation temperature are shown in **Fig. 3**. Average grain size is only increased from 10 μm to 15 μm with increasing welding simulation temperature from 1 200°C to 1 300°C. This can be attributed to the Nb-rich MX particles which inhibit the growth of the prior austenite grains up to about 1 285°C. Also, when the T/P92 steel is exposed at 1 300°C, δ-ferrite exists, as shown in Fig. 3(b), and the measured phase fraction of δ-ferrite at room temperature is about 6%.

Figure 4 shows results of tensile test at 750°C and fracture mode of the T/P92 steel depending on peak temperature. As shown in Fig. 4(a), regardless of the welding simulation peak temperature, the T/P92 steel shows large strains more than 55% and strain softening. Because the annihilation of dislocation and recovery of substructure are assisted by the deformation at high temperature,[1] the fracture mode of the welding-simulated T92 steels is totally ductile in Figs. 4(b) and 4(c). They show high RA values more than 70%, as shown in **Fig. 5**(a). In Fig. 5(b), the phosphorus segregation concentrations at grain boundaries

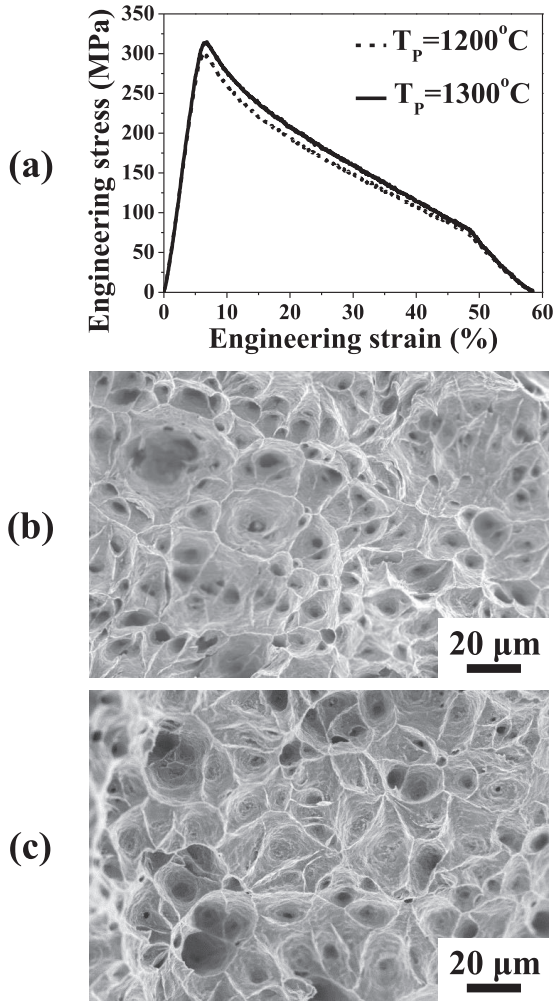

Fig. 4. Tensile test results at 750°C and the corresponding fracture surfaces of welding-simulated specimens: (a) tensile test results of T/P92, (b) fractograph of T/P92 with a peak temperature of 1 200°C and (c) fractograph at 1 300°C. Here, T_P is peak temperature of the welding simulation.

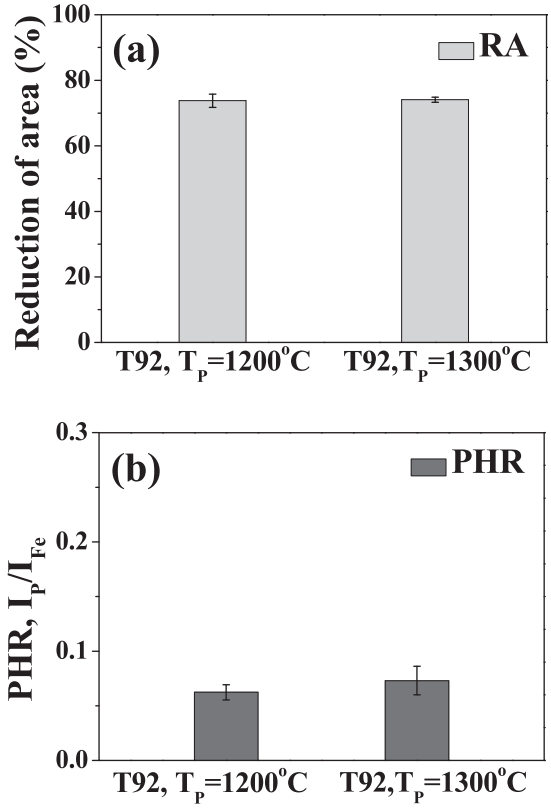

Fig. 5. The correlation between reduction of area (RA) and phosphorus segregation concentration: (a) RA of T/P92 and (b) peak height ratio (PHR) of phosphorus in T/P92.

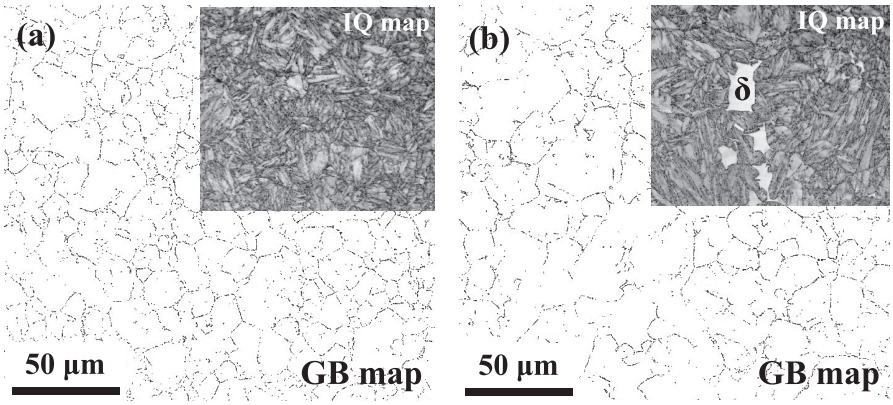

Fig. 3. Image quality (IQ) maps and grain boundary (GB) maps showing the boundaries with rotation angle from 15° to 45° of specimens after welding simulation in T/P92 steel: (a) peak temperature of 1 200°C and (b) 1 300°C.

of the T/P92 steel are very low and nearly similar at each welding simulation temperature.

Moreover, the ultimate tensile strength (UTS) of Fig. 4(a) is higher in the T/P92 steel with welding simulation at 1 300°C than at 1 200°C, even though the average grain size is larger at the higher welding simulation temperature. As shown in **Fig. 6**, martensite has the higher carbon content than the δ-ferrite, because the solubility of carbon in austenite is higher than that in δ-ferrite in 9Cr heat-resistant steels.[25] Therefore, the formation of δ-ferrite within the prior austenite grains can produce the higher average Vickers hardness (H_V 470) of the martensite matrix after the welding simulation at 1 300°C than that (H_V 459) after the welding simulation at 1 200°C. This is because the strength of martensite increases with increasing carbon content.[26] Consequently, the UTS is rather higher at the higher welding simulation temperature, as shown in Fig. 4(a).

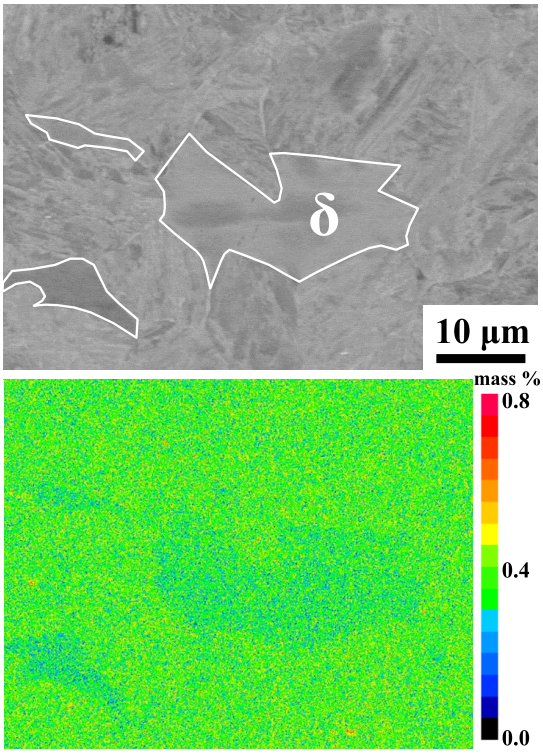

Fig. 6. Back-scattered electron (BSE) image and carbon distribution in welding-simulated T/P92 specimen with a peak temperature of 1 300°C. (Online version in color.)

4. Discussion

A previous study[23] which investigated reheat cracking in the T/P23 heat-resistant steel has suggested that this steel is susceptible to reheat cracking due to the active phosphorus segregation at PAGBs. The prior austenite grain size is about 110 μm when the steel was exposed to the welding simulation at 1 300°C, as shown in **Fig. 7**(b). The average grain size of the welding-simulated T/P92 steel is much smaller than that of the T/P23 steel. As shown in Figs. 3(a) and 7(a), grain size in the T/P23 steel exposed to the welding simulation at 1 200°C, about 50 μm, is also much larger than that in the T/P92 steel exposed to same peak temperature. This is because all precipitates hindering grain growth in the T/P23 steel are dissolved into the matrix below 1 200°C during the welding simulation, based on calculation in previous research.[27]

Changes in segregation concentration of phosphorus with grain size are calculated by the formula suggested by McLean[28] and Ishida[24] and this calculation can be applied to this research because segregating solute is only phosphorus and system in this study doesn't show any precipitation reactions directly related to the segregating phosphorus. The equilibrium phosphorus segregation concentration is expressed by

$$\frac{x^P}{1-x^P} = \frac{{}^o x - \frac{3t}{2\bar{R}} x^P}{1-{}^o x} \exp\left(\frac{-\Delta G_P^s}{RT}\right) \quad \text{..... (1)}$$

where x^P and ${}^o x$ are the phosphorus concentration at the grain boundary and the bulk concentration of phosphorus, respectively. $\bar{R}$ is the average grain radius and t is the grain boundary thickness assumed to be 1 nm.[24] R is the universal gas constant (8.314 J/mol·K) and ΔG_P^s is the free energy of segregation which is formulated by

$$\Delta G_P^s = -34\,300 - 21.5T \text{ (J / mol)} \quad \text{..... (2)}$$

where T is temperature in Kelvin.[29] ΔG_P^s is −56.298 kJ/mol at 750°C. In order to compare calculation and experimental results, the atomic fraction of phosphorus at grain boundaries from AES results can be estimated by

$$C_P = \frac{H_P/S_P}{\sum_k H_k/S_k} \quad \text{..... (3)}$$

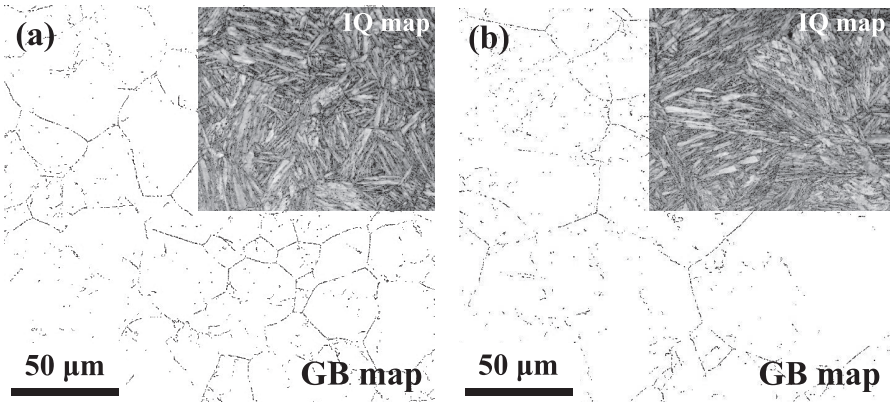

Fig. 7. IQ maps and GB maps showing the boundaries with rotation angle from 15° to 45° of specimens after welding simulation in T/P23 steels with phosphorus content of 0.01 wt.%: (a) peak temperature of 1 200°C and (b) 1 300 °C

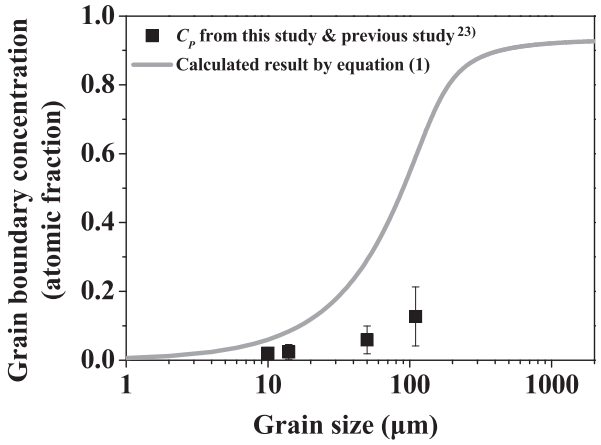

Fig. 8. Effect of grain size on phosphorus segregation concentration along grain boundary at 750°C.

where H is the Auger peak height from experiments and S is the sensitivity factor. The sensitivity factors of S_{Fe}, S_P are 0.205 and 0.613, respectively,[30] and the evaluated results are shown in **Fig. 8**. The grain boundary segregation concentration of phosphorus increases with increasing grain size. This is because the decrease in total grain boundary area with increasing grain size increases the equilibrium grain boundary segregation concentration of phosphorus at a given phosphorus bulk content. Therefore, the intergranular fracture behavior only in the T/P23 steel is mainly attributed to the much larger grain size which causes the much higher phosphorus segregation concentration during the tensile test at 750°C. Even though the experimental results are lower than the calculation results showing the equilibrium phosphorus segregation concentration at grain boundaries, due to a very short time for reaching the equilibrium segregation concentration, both results have a similar trend which shows abrupt increase in phosphorus segregation concentration, when the prior austenite grain size is higher than about 40 μm.

Finally, the inhibition of prior austenite grain growth by the undissolved Nb-rich carbo-nitrides during the welding simulation produces the much smaller prior austenite grain size in the T/P92 steel. Therefore, the insensitivity to intergranular cracking of the T/P92 steel is mainly attributed to the much lower phosphorus segregation concentration at the grain boundaries during tensile test at 750°C which results from the smaller prior austenite grain size.

5. Conclusions

(1) After the exposure to a severe welding thermal cycle, MX carbo-nitrides in T/P23 heat-resistant steels are dissolved, but not in T/P92 steels, due to the higher niobium and nitrogen contents. Therefore, even though the peak temperature of welding thermal cycle is same, the T/P23 steels show the much larger prior austenite grain size than the T/P92 steels. This is because the austenite grain growth is effectively interrupted by the Nb-rich MX carbo-nitrides during exposure to welding cycle.

(2) The calculation result showing changes in segregation concentration of phosphorus with grain size confirms that the phosphorus segregation concentration increases with increasing prior austenite grain size. In particular, it predicts that the phosphorus segregation concentration abruptly increases when the grain size is larger than about 40 μm. This trend is consistent with experimental results. Therefore, the T/P23 heat-resistant steels with the larger grain size are highly susceptible to reheat cracking, because of the severe phosphorus segregation at grain boundaries.

(3) T/P92 heat-resistant steels show a low phosphorus segregation concentration at grain boundaries, because of the much smaller grain size than the T/P23 steels after the welding cycle exposure. Also, these steels contain δ-ferrite due to the high chromium content after the exposure to a peak temperature of 1 300°C, but this phase doesn't have a detrimental effect on the cracking susceptibility. Therefore, T/P92 heat-resistant steels, which show ductile fracture with a high RA, are not susceptible to reheat cracking, regardless of the peak temperature of welding cycle.

Acknowledgments

The authors thank Korea Institute of Energy Technology Evaluation and Planning (Project No: 20152010103430) for the financial support and Mrs. Jung Hyun Yoon in Korea Institute of Science and Technology for the AES analysis.

REFERENCES

1) F. Abe, T. U. Kern and R. Viswanathan: Creep Resistant Steels, Woodhead Publishing, Cambridge, UK, (2008), 486.
2) A. Dhooge and J. Vekeman: *Weld. World*, **49** (2005), 75.
3) M. W. D. Van Der Burg, E. Van Der Giessen and R. C. Brouwer: *Acta Metall.*, **44** (1996), 505.
4) R. Raj: *Acta Metall.*, **26** (1978), 995.
5) D. Hull and D. E. Rimmer: *Philos. Mag.*, **4** (1959), 673.
6) M. V. Speight and J. E. Harris: *Met. Sci.*, **1** (1967), 83.
7) Y. J. Jin, H. Lu, C. Yu and J. J. Xu: *Mater. Charact.*, **84** (2013), 216.
8) J. G. Nawrocki, J. N. Dupont, C. V. Robino and A. R. Marder: *Weld. J.*, **79** (2000), 355.
9) J. G. Nawrocki, J. N. Dupont, C. V. Robino, J. D. Puskar and A. R. Marder: *Weld. J.*, **82** (2003), 25.
10) C. A. Hippsley, J. F. Knott and B. C. Edwards: *Acta Metall.*, **28** (1980), 869.
11) R. Raj and M. F. Ashby: *Acta Metall.*, **23** (1975), 653.
12) T. J. Chuang, K. I. Kagawa, J. R. Rice and L. B. Sills: *Acta Metall.*, **27** (1979), 265.
13) J. Shin and C. J. McMahon Jr.: *Acta Metall.*, **32** (1984), 1535.
14) D. Bika, J. A. Pfaendtner, M. Menyhard and C. J. McMahon, Jr.: *Acta Metall. Mater.*, **43** (1995), 1895.
15) C. A. Hippsley, J. F. Knott and B. C. Edwards: *Acta Metall.*, **30** (1982), 641.
16) W. T. Geng, A. J. Freeman and G. B. Olson: *Solid State Commun.*, **119** (2001), 585.
17) D. Y. Lee, E. V. Barrera, J. P. Stark and H. L. Marcus: *Metall. Trans. A*, **15** (1984), 1415.
18) Y. Q. Weng and C. J. McMahon, Jr.: *Mater. Sci. Technol.*, **3** (1987), 207.
19) N. H. Heo, J. C. Chang, K. B. Yoo, J. K. Lee and J. Kim: *Mater. Sci. Eng. A*, **528** (2011), 2678.
20) N. H. Heo and S.-J. Kim: *Mater. Sci. Eng. A*, **556** (2012), 533.
21) N. H. Heo, J. C. Chang and S.-J. Kim: *Mater. Sci. Eng. A*, **559** (2013), 665.
22) H. J. Sung, N. H. Heo, Y.-U. Heo and S.-J. Kim: *Mater. Sci. Eng. A*, **619** (2014), 146.
23) H. J. Sung, N. H. Heo and S.-J. Kim: *Metall. Mater. Trans. A*, **47** (2016), 1975.
24) K. Ishida: *J. Alloys Compd.*, **235** (1996), 244.
25) P. Mayr: Doctoral thesis, Graz University of Technology, Austria, (2007).
26) P. G. Winchell and M. Cohen: *Trans. ASM*, **55** (1962), 347.
27) H. J. Sung, N. H. Heo and S.-J. Kim: *Met. Mater. Int.*, **22** (2016), 962.
28) D. McLean: Grain Boundaries in Metals, Oxford University Press, London, (1957).
29) H. J. Grabke: *ISIJ Int.*, **29** (1989), 529.
30) K. D. Childs, B. A. Carlson, L. A. LaVanier, J. F. Moulder, D. F. Paul, W. F. Stickle and D. G. Watson: Handbook of Auger Electron Spectroscopy, 3rd Ed., Physical Electronics, MN, USA, (1995), 17.